Multispectral system for reflectance reconstruction in the near-infrared region

Meritxell Vilaseca, Jaume Pujol, Montserrat Arjona, and Marta de Lasarte

We analyze the performance of a multispectral system that works in the near-infrared (NIR) region of the electromagnetic spectrum (NIR: 800–1000 nm). The system, which uses a CCD camera as a sensor with five acquisition channels, is capable of reconstructing the NIR spectral reflectance curves for a wide range of samples with a high degree of accuracy. We carried out a study of the sources of error in the experimental system, developed a luminance adaptation model to remove the dependence of the captured images on the exposure time of the camera and the *f*-number of the objective lens, and performed reconstructions of the spectral reflectances of a set of 80 samples. We achieved the best results by using a 12-bit camera, considering a different luminance adaptation transform for each channel, and by using the pseudoinverse reconstruction method. Under these conditions, the system provided mean percentages of reconstruction higher than 99.8% and root-mean-square-error values lower than 0.17, and is therefore suitable for use as a spectrophotometric instrument.

OCIS codes: 040.1520, 110.3080, 110.4190, 300.6340, 350.2460, 350.4600.

1. Introduction

In this study we analyze the experimental performance of a multispectral system, which was developed to obtain the reflectance spectra of samples in the near-infrared (NIR) region of the electromagnetic spectrum (NIR: 800–1000 nm) as a continuation of work undertaken in previous studies.[1–4] Up to now, conventional multispectral imaging systems[5,6] have mainly been used in applications that involve the measurement of visible light. These systems have started to be used in many different fields, such as the conservation of paintings,[7,8] color reproduction,[9–11] e-commerce, and telemedicine.[11] However, their use in other parts of the electromagnetic spectrum is still uncommon. The multispectral system developed in this study consists of an illumination system used to light the samples that emit a considerable amount of NIR radiation, five spectral bands composed of interference filters with different transmittance profiles in the NIR, and a digital CCD camera attached to an automated zoom lens. Because of the difference in spectral sensitivity of the NIR multispectral channels, it was possible to obtain spectral information on the samples analyzed in the spectral range considered.

Because the spectral information in the NIR is related to the chemical properties of the materials, it is used as an analytical tool known as NIR technology.[12–14] In the NIR, there are absorption peaks resulting from the vibrations of molecules that are present in the materials, such as biological substances (e.g., proteins, fiber, moisture, and fats) and other chemical constituents (such as those that are present in textiles, plastics, and petrochemical products). Although these spectral bands are usually highly overlapped, to overcome this limitation the NIR technology relates the spectra of the objects analyzed to the corresponding chemical components with the use of complex multivariate mathematics, so that they can be identified.[12] This technology has a wide range of applications and is used in areas such as agriculture, food and pharmaceutical analysis, and the textile, paint, chemical, and petrochemical industries. The multispectral system developed in this work is capable of reconstructing NIR spectra with a certain degree of smoothness, as is typical in these kinds of systems. Taking into account that the NIR absorption peaks are usually overlapped and therefore that the associated spectra are quite smooth, the multispectral system developed can be used as an auxiliary tool in NIR technology, and some of the properties of the samples analyzed with peaks in the

The authors are with the Center for Sensors, Instruments and Systems Development, Department of Optics and Optometry, Technical University of Catalonia, Rambla Sant Nebridi 10, 0822 Terrassa, Spain.

Received 2 September 2005; revised 1 December 2005; accepted 6 December 2005; posted 8 December 2005 (Doc. ID 64614).

0003-6935/06/184241-13$15.00/0

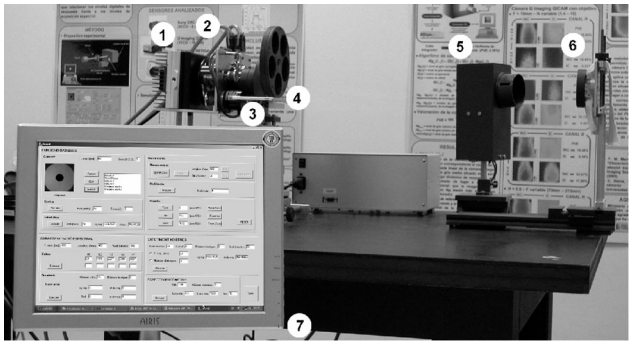

Fig. 1. Experimental setup of the NIR multispectral system: 1, CCD camera; 2, automated zoom lens; 3, cutoff infrared and visible filters; 4, multispectral filters wheel; 5, halogen lamp; 6, sample support; 7, personal-computer unit and developed software interface.

considered range can be deduced from the information that is available instead of using conventional spectrophotometers, which are commonly employed for this purpose. Furthermore, commercial spectrophotometers for NIR applications usually use a diffraction grating and more specific detectors such as InGaAs or PbS,[12] which can be relatively expensive.

The system uses a CCD camera[15] as a sensor. CCD cameras are commonly used in areas such as image processing and artificial vision and in more specific fields such as photometry or radiometry, many of which are still in their experimental stages. They are used for these applications because their maximum spectral response is within the visible region, that is, between 380 and 780 nm. However, CCD sensors are still highly sensitive in the NIR, and CCD cameras with improved response in the NIR have recently appeared on the market. Furthermore, CCD cameras are composed of an array of sensors and can therefore obtain high-resolution information from many parts of the image simultaneously, which is a major advantage over conventional spectrophotometers. Therefore, in this paper, we propose the use of CCD cameras for NIR measurements. Both 8-bit and 12-bit cameras were analyzed to obtain good spectral reflectance reconstructions of the samples.

To reconstruct the spectral reflectance curves, several multispectral images were acquired through the system's various acquisition channels. In previous studies,[1–3] five channels were found to provide optimum results in the NIR. Subsequently, a luminance adaptation model[3,16] was applied to the images to free them from their dependency on the exposure time (t_{exp}) of the camera and the f-number (N) of the zoom lens. These two parameters expand the dynamic range of the camera along which the measurements can be made, and therefore different amounts of radiation can be measured.

Once the images had been corrected by the luminance adaptation model, several mathematical algorithms were used to recover the reflectance spectra of the samples analyzed from the multispectral measurements performed. In previous research[1–3] we analyzed several methods of reconstruction by numerical simulation, some of which were based on interpolation algorithms and others on more accurate estimation techniques; we determined that the best results were given by the latter methods, particularly by pseudoinverse estimation[2,17] (PSE), a nonlinear estimation[18–20] (NLE) method that uses a second-order polynomial, and principal-component analysis[21,22] (PCA). In this study we analyze the capacity of these three methods to reconstruct spectral reflectances in the NIR.

Finally, the NIR multispectral system developed was used to study a wide range of representative samples, including natural and manufactured objects. Because of the different composition of these materials, they tend to exhibit different behaviors from a spectral point of view in the presence of NIR radiation, although their reflectance profiles are typically smooth. The samples included materials such as textiles, plastics, marble, paper, cardboard, wood, plants, and leather, and different kinds of food such as cheese, bread, crackers, meat, vegetables, and fruit. The results of the reconstruction show the potential of the proposed method and the usefulness of the system for obtaining information on the reflectance of the samples.

The paper is structured as follows. Section 2 describes the experimental setup, the luminance adaptation model and the spectral reconstruction method. Section 3 presents a summary of the results, with a preliminary study of the sources of error that affect the system and the experimental reconstructions obtained with 8-bit and 12-bit cameras. Finally, the most relevant conclusions are discussed in Section 4.

2. Method

A. Experimental Setup

The experimental setup of the multispectral system (Fig. 1) consisted of a halogen lamp (Philips 15V 150W, $T_c = 3357$ K) (see Fig. 2), which emitted a considerable amount of light in the NIR interval studied and was connected to a Hewlett Packard 6642A dc power supply for the stable illumination of the sample; a wheel with five interference filters (ThermoCorion) with a full-width half-maximum (FWHM) of ~70 nm and equispaced transmittance peaks in the NIR (Fig. 3); two more filters (a cutoff infrared filter and a cutoff visible ThermoCorion filter) to ensure that the radiation reaching the sensor came only from the NIR range considered (Fig. 4); and finally a CCD camera attached to an automated objective lens (Cosmicar Pentax C6Z1218M3-1 12.5–75 mm).

The automated zoom lens provided accurate control over the focus, zoom, and iris (f-number). Often the manual mechanical positioning of these factors in conventional objectives does not guarantee high precision, so highly consistent measurement conditions are not achieved. Because multispectral systems are to a certain degree affected by the errors present, to

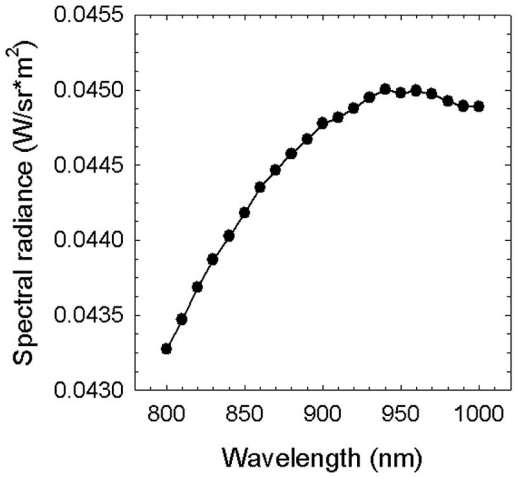

Fig. 2. Spectral radiance emitted by the halogen lamp in the NIR region.

achieve good reconstructions the zoom lens had to be motorized.

Two different types of CCD camera were tested for use in the NIR multispectral system: a Hamamatsu C7500-51 with improved response in the NIR and 8-bit depth and a Photometrics Sensys KAF0400-G2 with 12-bit depth. The spectral sensitivities of both cameras are shown in Fig. 5. The spectral features of the emission of the halogen lamp and the transmittance of the filters, as well as the number of channels used in the system, were chosen according to the results obtained in previous studies,[1–3] in which several simulations were performed to optimize the reconstructions in the NIR.

B. Luminance Adaptation Model

The experimental system described above allows us to obtain five multispectral images of the samples we analyzed through the acquisition channels by using

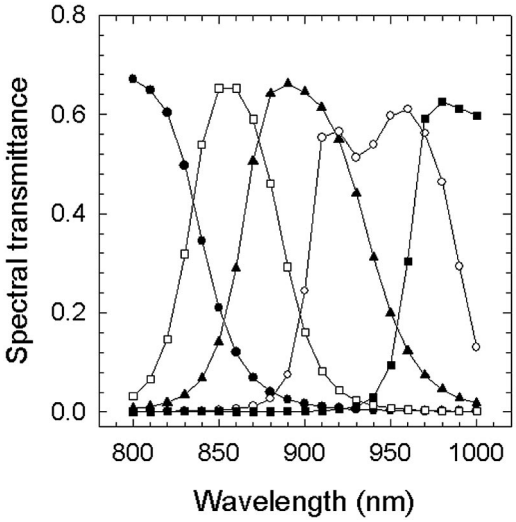

Fig. 3. Transmittance of the five multispectral filters in the NIR region. The corresponding peak wavelengths are F1, 800; F2, 860; F3, 890; F4, 960; and F5, 980 nm.

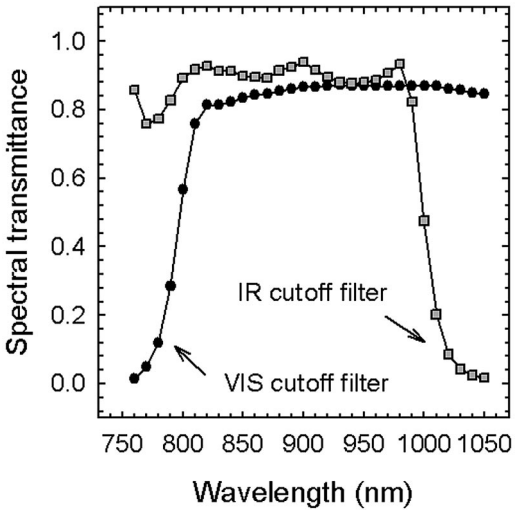

Fig. 4. Transmittance of the cutoff visible and infrared filters in the NIR region.

different exposure time values for the camera (t_{exp}) and different f-numbers for the zoom lens (N). The variability of these parameters is useful since it allows us to adapt the dynamic range of the sensor to the amount of incident light and therefore to measure a wide range of inputs with different luminous features, obtaining digital levels centered within the linear range of the camera for each acquisition channel. The camera responses are highly dependent on the channel that is used because of the different transmittances of the multispectral filters and the typically decreasing profile of the spectral sensitivity of the CCD sensor in the NIR.

To free the images acquired from dependence on the exposure time and f-number, it was necessary to develop a luminance adaptation model. The model developed in this work transforms the measured camera responses or digital levels for each t_{exp} and N value into theoretical camera responses. The theoretical camera responses are independent of both parameters and may be calculated as follows:

$$X_i = \int_{\lambda_{min}}^{\lambda_{max}} i(\lambda) r(\lambda) F_i(\lambda) S(\lambda) d\lambda, \quad (1)$$

where X_i is the theoretical camera response obtained for a certain channel ($i = 1, \ldots, 5$), $i(\lambda)$ is the spectral radiance of the lamp, $r(\lambda)$ is the measured spectral reflectance of the sample, $F_i(\lambda)$ is the spectral transmittance of the filters, and $S(\lambda)$ is the spectral sensitivity of the CCD camera used.

The model developed applies a linear correction to the digital levels measured [$DL(t_{exp}, N)$] and transforms them into theoretical camera responses (X_i). In the literature, only one theoretical model[16] that uses optoelectronic conversion functions (OECFs) was found.

We calculated the transformations corresponding to the luminance adaptation model for each of the

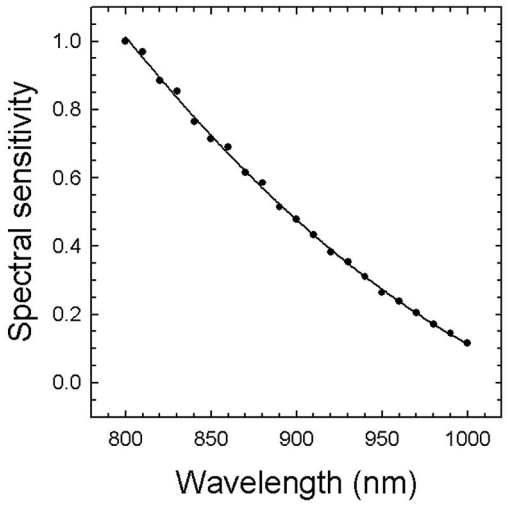

(a)

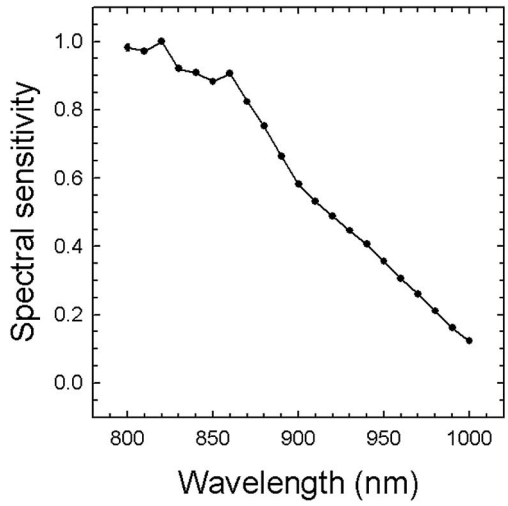

(b)

Fig. 5. Spectral sensitivity of the cameras used in the experimental setup: (a) Hamamatsu C7500-51 and (b) Photometrics Sensys KAF0400-G2.

(t_{exp}) and N values by taking into account a set of reference samples of known spectral reflectance in the NIR, measured by means of a telespectrophotometer (Instrument Systems Spectro 320), and we obtained them by fitting the normalized digital levels [NDL(t_{exp}, N)] to the theoretical camera responses (X_i). These kinds of regressions are referred to as type 1 transformations. We performed the linear fittings for a wide range of exposure times (t_{exp}) and f-numbers (N). Because the zoom lens was motorized, the f-numbers provided (N^*) are not the real f-numbers but instead correspond to a specific position of the motor that controls the automated iris of the zoom. These positions may vary from 0 (equivalent to an f-number of 1.4) to 1750 (equivalent to a completely closed iris), increasing in steps of 1. The values tested for t_{exp} were 10, 20, 40, 70, 100, 150, 200, 300, 400, and 500 ms (maintaining $N^* = 550$), and for N^*, 100, 200, 300, 400, 500, 600, 700, 800, 900, and 1000 (maintaining $t_{exp} = 100$ ms). An example of a correction obtained for $t_{exp} = 20$ ms and $N^* = 550$ is given in Fig. 6. Table 1 shows the parameters for the correction, that is, the slope value (m), the offset value (n), and the regression coefficient r.

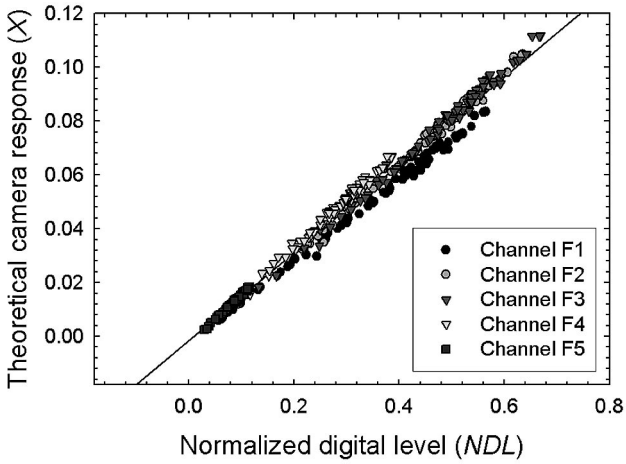

Fig. 6. Luminance adaptation correction obtained for $t_{exp} = 20$ ms and $N^* = 550$ with type 1 transformation.

For each pair of parameters (t_{exp}, N^*), a different linear transformation was found. The slope value of the transformations corresponded to a scale factor that was necessary for readjusting the responses and to treat them in absolute terms of energy. This was because the amount of light reaching the CCD sensor depended on the exposure time and f-number and also because in the theoretical camera responses we considered the spectral radiance of the halogen lamp instead of the exposure reaching the sensor; likewise, the spectral sensitivity of the camera was expressed in relative terms. The offset value was an uncontrollable correction factor that was due to experimental errors and noise. It presented a random value close to 0.

Another kind of fitting that can also be performed to correct multispectral images is to take into account a different transformation depending on the acquisition channel considered, in addition to the exposure times and f-numbers. These kinds of association, which are referred to as type 2 transformations, allowed us to take into account the influence of the wavelength on the f-number and to better compensate for several systematic errors in the system that affected the multispectral bands. Examples of these errors include the approximations performed in the outermost channels, corresponding to filters F1 and F5, in which we considered that all the energy that did not come from the spectral interval (800–1000 nm) was removed by using the cutoff filters (which was not exactly true because of their transmittance curves) and the lower sensitivity of the spectral bands of longer wavelengths that was due to the decreasing profile in the spectral response of the camera in the NIR [which may cause these channels to

Table 1. Correction Parameters of the Luminance Adaptation Model Obtained for t_{exp} = 20 ms and N^* = 550 with Transformations 1 and 2

Transformation	Channel	Slope Value (m)	Offset Value (n)	Coefficient (r)
Type-1	—	0.1634	−1.7303e-3	0.9932
Type-2	F1	0.1523	−2.9010e-3	0.9980
	F2	0.1707	−4.2451e-3	0.9979
	F3	0.1739	−5.2970e-3	0.9972
	F4	0.1830	−3.8571e-3	0.9965
	F5	0.1815	−2.9184e-3	0.9955

have a lower signal-to-noise ratio (SNR)]. Therefore subsequent reconstructions were more accurate if the corrections were performed with these transformations, that is, independently for each channel. An example of a type 2 transformation is shown in Fig. 7. The corresponding slope values (m), offset values (n), and regression coefficients (r) are listed in Table 1. As can be seen, in most cases, the regression parameters we obtained by using these corrections are better than those we obtained with type 1 transformations, and therefore the reconstructions are expected to be more accurate using these corrections.

Finally, the slope values can be modeled with the exposure time for a constant f-number and, similarly, they can be modeled with the f-number for each exposure time. This is accomplished for transformations of types 1 and 2, in the latter case by the consideration of each channel independently. The best fitting functions encountered correspond to quadratic regressions and can be expressed as follows:

$$\text{Exposure time } (t_{\text{exp}}): \quad m = 1/(a + bt_{\text{exp}} + ct_{\text{exp}}{}^2) \quad (N = \text{constant}),$$

$$f\text{-number } (N^*): \quad m = 1/(a + bN^* + cN^{*2}) \quad (t_{\text{exp}} = \text{constant}). \tag{2}$$

The prediction of the slope values by means of these fittings is very useful because the luminance adaptation model can be extrapolated for exposure times and f-numbers that have not been experimentally measured. Moreover, we did not find any simple fitting function for the offset parameter and the exposure time or the f-number position. This is because this parameter is related to experimental errors and has a random value, so it cannot be modeled. However, it can be rejected because of its insignificant value. Specific examples of these regressions can be seen in Figs. 8 and 9.

C. Spectral Reconstructions

Once the digital levels measured have been corrected with the luminance adaptation model, they can be inserted into a reconstruction algorithm to recover the spectral reflectance profile of the sample analyzed. In this study, we applied three different mathematical reconstruction methods, PSE, NLE, and PCA, and compared their performance in the NIR. All three algorithms use a training set of known spectral reflectances to perform the reconstructions.

The PSE and NLE methods reconstruct the spectral reflectance curves from the camera responses using a transformation matrix that is calculated as follows:

$$\tilde{\mathbf{r}} = \mathbf{M}_T \cdot \mathbf{X} = \mathbf{O}_r\mathbf{X}_{\mathrm{O}_r}{}^T\left(\mathbf{X}_{\mathrm{O}_r}\mathbf{X}_{\mathrm{O}_r}{}^T\right)^{-1} \cdot \mathbf{X}, \tag{3}$$

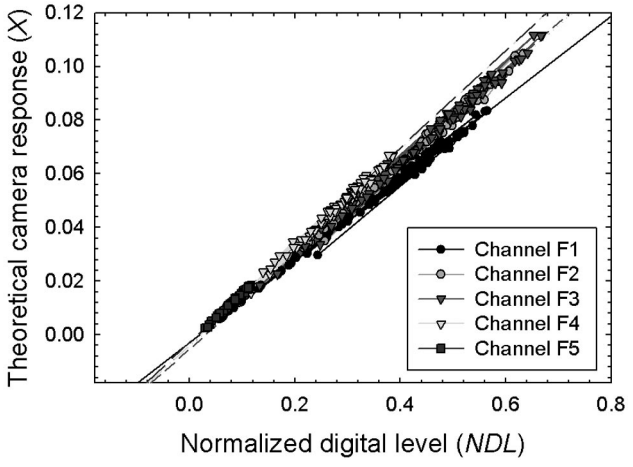

Fig. 7. Luminance adaptation correction obtained for t_{exp} = 20 ms and N^* = 550 with type 2 transformation.

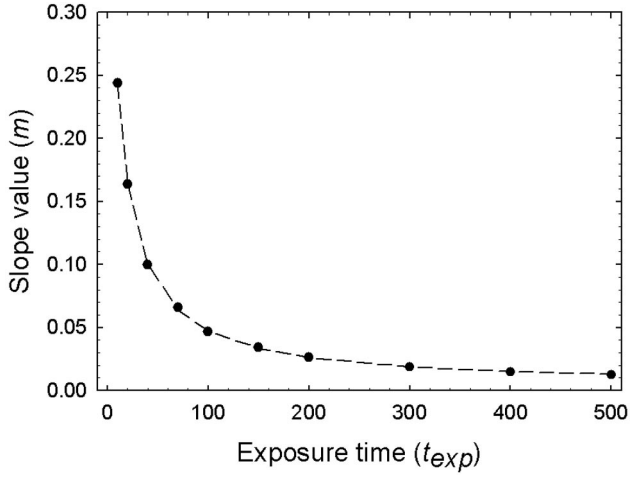

Fig. 8. Quadratic regression between the slope value and the exposure time for type 1 transformations (N^* = 550).

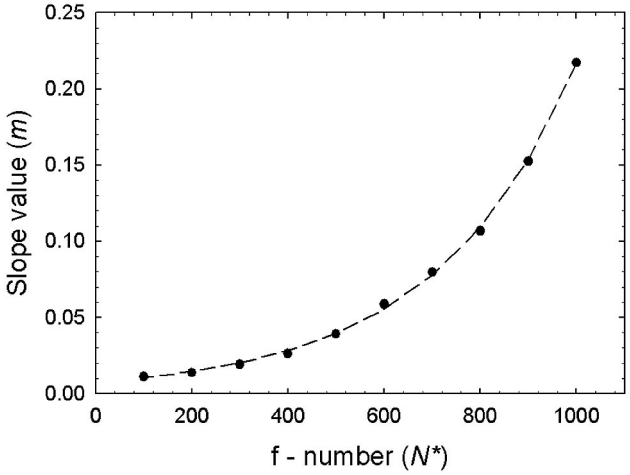

Fig. 9. Quadratic regression between the slope value and the *f*-number position for type 1 transformations (t_{exp} = 100 ms).

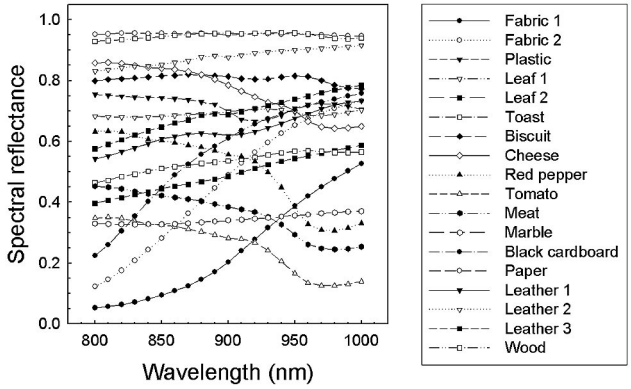

Fig. 10. Spectral reflectances in the NIR region of some analyzed samples measured with the telespectrophotometer.

where $\tilde{\mathbf{r}}(n \times 1)$ is a column vector representing the spectral reflectance of the sample evaluated at n wavelengths, $\mathbf{M}_T(n \times m)$ is the transformation matrix, and $\mathbf{X}(m \times 1)$ is a column vector representing the camera responses for the m multispectral channels of the sample (X_i). $\mathbf{O}_r(n \times p)$ is a matrix whose columns are the known spectral reflectances of the samples belonging to the considered training set evaluated at n wavelengths. For the PSE method $\mathbf{X}_{O_r}(m \times p)$ is a matrix whose columns contain the camera responses for the m multispectral channels belonging to the p samples of the training set. On the other hand, for the NLE method the columns of $\mathbf{X}_{O_r}$ are polynomial combinations of the m camera responses of the p samples, and therefore the number of rows of the matrix depends on the polynomial used.

Specifically, for PSE and NLE, the $\mathbf{X}_{O_r}$ matrixes are as follows:

PSE:

$$\mathbf{X}_{O_r} = \begin{bmatrix} X_{1,1} & \cdots & X_{1,p} \\ X_{2,1} & \cdots & X_{2,p} \\ \vdots & & \vdots \\ X_{m,1} & \cdots & X_{m,p} \end{bmatrix},$$

NLE:

$$\mathbf{X}_{O_r} = \begin{bmatrix} 1 & \cdots & 1 \\ X_{1,1} & \cdots & X_{1,p} \\ X_{2,1} & \cdots & X_{2,p} \\ \cdot & & \cdot \\ X_{1,1}^2 & \cdots & X_{1,p}^2 \\ X_{2,1}^2 & \cdots & X_{2,p}^2 \\ \cdot & & \cdot \\ X_{1,1}X_{2,1} & \cdots & X_{1,p}X_{2,p} \\ \cdot & \cdots & \cdot \end{bmatrix}. \quad (4)$$

However, with the PCA technique, we obtain the spectral reflectance for each sample by combining the following expressions:

$$\mathbf{X} = \mathbf{C}r, \quad (5)$$

$$\tilde{\mathbf{r}} \approx \mathbf{r}_M + \alpha\mathbf{v}_{r1} + \beta\mathbf{v}_{r2} + \gamma\mathbf{v}_{r3} + \delta\mathbf{v}_{r4} + \cdots + \xi\mathbf{v}_{rq}, \quad q < n, \quad (6)$$

where $\mathbf{C}(m \times n)$ is a matrix whose rows are the spectral sensitivities for each multispectral channel, $\mathbf{r}_M$ is the mean spectral reflectance of the samples belonging to the training set, $\alpha, \beta, \ldots, \xi$ are scalar coefficients, and $\mathbf{v}_{r1}, \mathbf{v}_{r2}, \ldots, \mathbf{v}_{rq}$ are the principal components calculated with the training set.

We calculate the scalar coefficients for each sample analyzed by solving the system using as many principal components as the number of multispectral channels used in the reconstruction. Once the scalar coefficients are known, the spectral reflectance can be recovered.

For the methods tested, all of which can easily be implemented with the commercial MATLAB software, we performed the reconstructions by using two to five acquisition channels. The multispectral filters considered for the reconstructions with fewer channels than five were the following: two channels, F2, F4; three channels, F2, F3, F4; and four channels, F1, F2, F3, F4.

The reconstructions were carried out for a set of 80 different samples with different reflectance spectra in the NIR. The samples included natural and manufactured objects such as textiles, plastics with different compositions, marble, different kinds of wood and paper, plants, leather, and food (e.g., cheese, bread, crackers, meat, vegetables, and fruit). Several examples of the reflectance spectra of the samples measured with the telespectrophotometer (Instrument Systems Spectro 320) are shown in Fig. 10. The telespectrophotometer integrated the data over a region of 0.5 cm in diameter, where the samples presented fairly constant features and the illumination was uniform. An area of approximately 8000 pixels over the sensor, equivalent to the zone measured with the telespectrophotometer, was used to obtain the averaged digital levels of each analyzed sample.

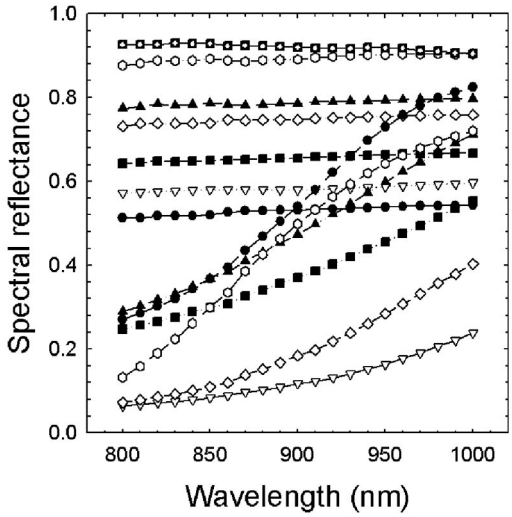

Fig. 11. Spectral reflectances in the NIR region of some of the 19 textile samples considered in the simulations measured with the telespectrophotometer.

To evaluate the quality of the reconstructed spectra, we used the following two parameters:

- percentage of reconstruction:

$$P_{\mathrm{rec}} = \left[1 - \frac{\sum_{\lambda_{\min}}^{\lambda_{\max}} (r - \tilde{r})^2}{\sum_{\lambda_{\min}}^{\lambda_{\max}} (r)^2}\right] \times 100, \tag{7}$$

- root-mean-square error[23,24] (RMSE):

$$\mathrm{RMSE} = \left[\frac{1}{N_\lambda} \sum_{\lambda_{\min}}^{\lambda_{\max}} (r - \tilde{r})^2\right]^{1/2}, \tag{8}$$

where r are the experimentally measured components of the reflectance curves, $\tilde{r}$ are the reconstructed values, and N_λ is the number of wavelengths in which the measurements were taken. In this study the measurements and reconstructions are performed with a wavelength step of 10 nm so that N_λ is always considered 21.

While the RMSE is a commonly used parameter in multispectral imaging and its value is related to the distance between the measured and reconstructed spectra, P_{rec} provides an intuitive idea of the quality of the reconstruction, since its maximum value is 100. We have shown in previous works[1–3] that RMSE values similar to 0.01 and percentages of reconstruction close to 99.9% lead to almost perfect reconstructions of the NIR spectral reflectances of most samples.

3. Results

A. Analysis of the Sources of Error

Before performing the experimental reconstructions, we evaluated the different sources of error in the system developed. Only a few authors[25–27] have briefly analyzed the implications of these errors for reconstructions. Common sources of error found in conventional multispectral systems are the noise made by the CCD camera, the mechanical positioning of the elements, the oscillations in the emission of the illumination source, the different geometries used in the spectral measurements, and the mathematical approximations performed by the methods of reconstruction employed.

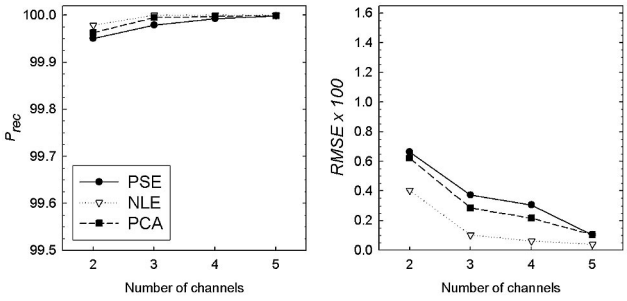

Fig. 12. Simulated results of reconstruction (mean P_{rec} and RMSE) obtained for the 19 textile samples without noise being introduced.

In this study, all the controllable experimental errors were reduced before the measurements were performed. We motorized the objective lens, and the errors introduced into the averaged camera responses by means of the zoom, focus, and iris changes had a standard deviation below 0.2%. The multispectral filters were mounted on a wheel, and a special support was built to hold the samples and thus guaranteed a high degree of precision in the mechanical positioning during the measurements. Furthermore, the halogen lamp was attached to a dc power supply to obtain a stable illumination of the samples analyzed. Its emission was temporally characterized, and the standard deviation associated with the mean radiance measured showed a variation of less than 0.5%. Another factor that must be taken into account is the geometry with which the measurements are taken. In some cases, the geometries used to determine the spectral reflectances of the samples with a conventional spectrophotometer and the multispectral acquisitions are different. In our case, the telespectrophotometer placed in the same position as the camera was used to measure the spectra.

Nevertheless, the methods of reconstruction are not exact because the methodologies used apply mathematical techniques that are approximative, such as the least-squares regression. Other more practical reasons included the fact that in the calculations associated with the process of reconstruction we considered only the wavelengths included in the 800–1000-nm range, although the cutoff filters did not completely remove all the radiation, and the fact that the theoretical calculations were performed with a wavelength step of 10 nm. We optimized this latter factor by taking into account the results we obtained by using other step values. Because of the high degree of smoothness of the spectral profiles of the samples in the NIR,[12] it was seen that 10 nm was enough to ensure highly accurate reconstructions.

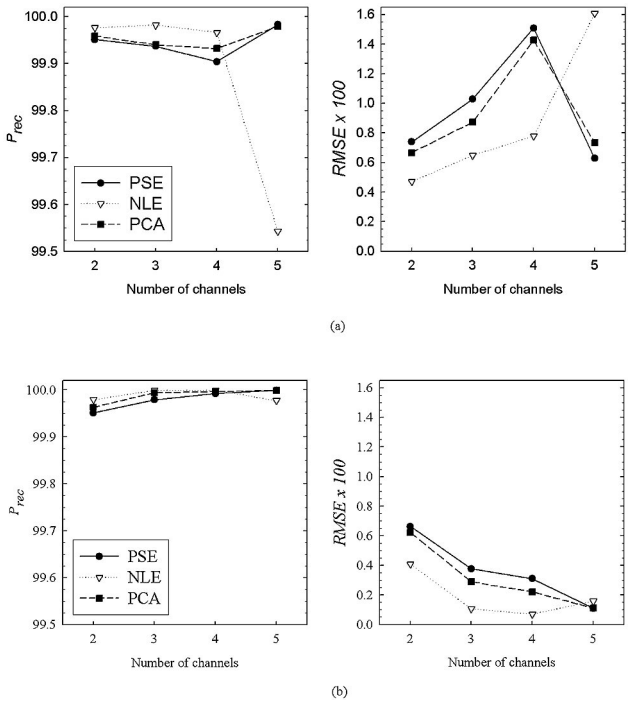

Fig. 13. Simulated results of reconstruction (mean P_{rec} and RMSE) obtained for the 19 textile samples introducing quantization noise corresponding to (a) 8 bits and (b) 12 bits.

Finally, we analyzed the errors introduced by the CCD cameras,[28,29] which are one of the most relevant sources of noise in multispectral systems. CCD cameras are affected by many different types of noise, of which the following three were studied: dark current, shot noise, and quantization noise. Because of the configuration of our experiment, the dark current was reduced by use of a cooling system when the 12-bit sensor was used. To take advantage of the entire dynamic range of the camera, we eliminated the dark-current image by changing the gain and offset parameters. We also minimized the shot noise by averaging several images for each acquisition performed. The quantization noise was analyzed with both 8-bit and 12-bit sensors.

To quantify the influence on the reconstructions of the different kinds of camera noise, simulations were carried out. First, simulations were performed on a set of only 19 textile samples to simplify the calculations. In Fig. 11 the most representative samples of this set can be seen. The samples that are not presented are very similar to those of some of the curves shown. Figure 12 shows the ideal mean P_{rec} and RMSE values for this set of samples that would be obtained with our system without noise. In this case, the reconstructions improved with the number of channels, as was expected, and they are highly accurate, with P_{rec} values higher than 99.9% and (RMSE $\times$ 100) values lower than 1. The best performing methods were NLE, PCA, and PSE respectively.

The influence of the quantization noise on the system was analyzed by the introduction of the corresponding errors in the simulations. To achieve this, the theoretical camera responses used in the simulations were transformed into digital levels by use of Eq. (9), and the quantization errors were subsequently introduced by means of the *integer* function:

$$\mathrm{DL}_i = \mathrm{integer}\left[X_i \frac{\mathrm{DL}_{\max}}{(X_i)_{\max}}\right], \tag{9}$$

where DL_i is the digital level for each channel and sample, X_i is the theoretical response of the camera, $\mathrm{DL}_{\max}$ is the maximum digital level corresponding to the number of bits used (255 for 8 bits and 4095 for 12 bits), and $(X_i)_{\max}$ is the theoretical response of the camera to an ideal sample with spectral reflectance 1 at all wavelengths. The *integer* function provides the closest integer number to the value we obtained by performing the mathematical operations.

Using the inverse transformation, we again obtained the theoretical camera responses affected by the error and carried out the corresponding reconstructions, Fig. 13 illustrates the results obtained. Table 2 shows the mean SNR [Eq. (10)] associated with the samples for each acquisition channel:

$$\mathrm{SNR}_i = 10 \log\left(|\mathrm{DL}_i|^2 / |\mathrm{DL}_{\mathrm{noise}\,i}|^2\right), \tag{10}$$

where $\mathrm{DL}_{\mathrm{noise}}$ is the increment or decrement of the digital level corresponding to the quantization noise.

PSE and PCA methods yielded very similar results. With 8-bit quantization noise, the reconstructions were worse when three and four channels were used than they were when two channels were used. This can be explained by the greater proportion of errors in the calculations when more channels are used and by the smoothness of the reflectances, which makes it possible to obtain good reconstructions by use of just a small number of bands. This behavior is eliminated when five channels are used because the errors are compensated for by the additional information. Conversely, with the NLE method, the reconstruction results always deteriorate with the number of filters used. This is true even in the case of five filters. The reason for this is that this method uses second-order polynomials of the camera responses, so the errors are amplified considerably. In conclusion, PSE and

Table 2. Mean Signal-to-Noise Ratio Obtained for the 19 Textile Samples Corresponding to Each Channel with Different Errors Introduced

SNR	F1	F2	F3	F4	F5
Quantization noise 8-bit	49.514	52.874	51.581	53.526	53.581
Quantization noise 12-bit	70.563	74.447	74.763	73.191	74.330
Proportional noise 1%	47.195	49.380	44.581	47.708	49.558
Proportional noise 0.5%	56.792	53.665	56.281	56.140	56.970

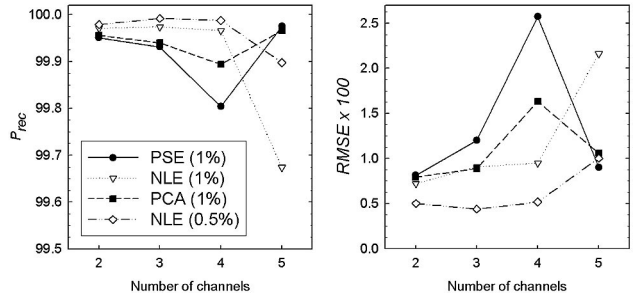

Fig. 14. Simulated results of reconstruction (mean P_{rec} and RMSE) obtained for the 19 textile samples when a proportional noise of 1% is introduced (and 0.5% in the case of the NLE method).

PCA methods are recommended when the reflectance spectra of samples with an 8-bit system are being recovered. Using these two methods and five channels, the reconstruction parameters fulfill the conditions imposed, that is, $P_{rec} \geq 99.9\%$ and (RMSE $\times$ 100) ≤ 1.

However, when a 12-bit quantization noise was included in the simulations, the results improved significantly and reconstruction parameters similar to the ideal ones and a higher SNR were achieved. In this case, the reconstructions always improved with the number of channels, except when the NLE method was used. With 12 bits, the reconstruction results verify the conditions imposed, even when fewer than five channels were used.

Finally, to simulate the shot noise of the camera and its influence on the reconstructions, an additive term that represented a percentage of the signal was introduced in the simulations:

$$X_i' = X_i + \varepsilon_i, \tag{11}$$

where X_i' are the camera responses affected by noise and ε_i is the proportional noise introduced. It was defined by use of the RAND function in MATLAB, which generates a random number between 0 and 1. For instance, a noise equivalent to 1% is introduced by the following expression:

$$\varepsilon_i = (0.02\ \text{RAND} - 0.01)X_i. \tag{12}$$

The reconstruction results obtained when this noise is introduced into the simulations is shown in Fig. 14, and the corresponding SNR is shown in Table 2. In this case, the SNRs obtained are even worse than when a quantization noise of 8 bits was introduced. This causes the reconstructions to behave in the same way: They deteriorate with three and four channels and improve with five channels, except in the case of the NLE method. When the PSE and the PCA methods and five channels are used, a shot noise lower than 1% guarantees that the reconstruction parameters will verify the conditions imposed [$P_{rec} \geq 99.9\%$, (RMSE $\times$ 100) ≤ 1]. For the NLE method, the noise must be lower than 0.5% to obtain these values.

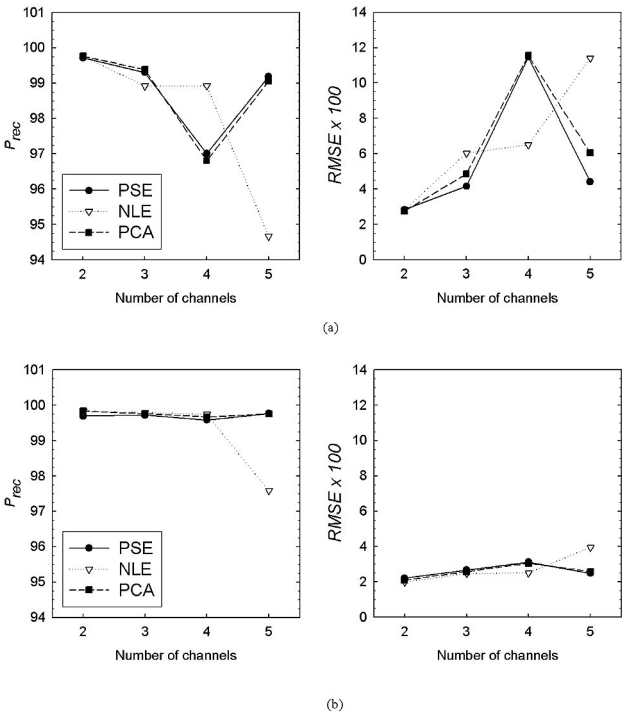

Fig. 15. Experimental results of reconstruction (mean P_{rec} and RMSE) obtained for the 19 textile samples with the 8-bit camera and the luminance adaptation model with (a) type 1 transformations and (b) type 2 transformations.

B. Reconstructions with 8-bit Cameras

In this section, we describe the experimental reflectance reconstructions with the multispectral system developed by using an 8-bit Hamamatsu C7500-51 camera, even though the simulated results obtained in the previous subsection were not optimal under these conditions. First, to carry out a straightforward test of the system, we also used a set of just 19 textile samples. The reconstructions were performed with the luminance adaptation model and transformations of types 1 and 2. For each sample, the most adequate *f*-numbers and exposure times were used, that is, those that provided digital levels within the linear range of the camera. The results obtained for the reconstructions are shown in Fig. 15. The results obtained with type-1 transformations were clearly worse than those obtained with type-2 transformations. With type 2, the experimental errors that variously affect the multispectral channels were better compensated for, so more accurate reconstructions were obtained. The methods behave in the same way as they did in the noise simulations, that is, PSE and PCA give worse results with three and four channels, but with five channels this tendency was eliminated. With NLE, the results always deteriorated when the number of channels increased. However, this tendency was significantly reduced with type-2 transformations. When PSE and PCA with five channels were used, the P_{rec} values were higher than 99.8% and the (RMSE $\times$ 100) values were lower than

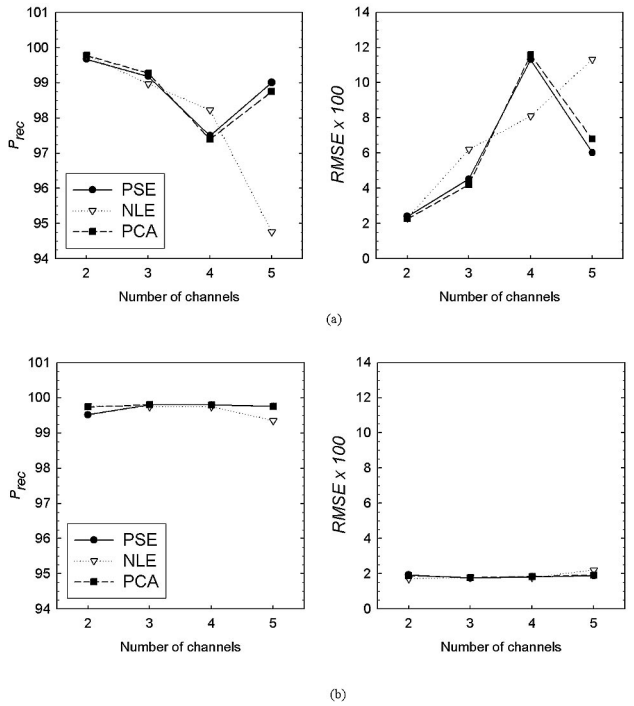

Fig. 16. Experimental results of reconstruction (mean P_{rec} and RMSE) obtained for the 19 textile samples with the 12-bit camera and the luminance adaptation model with (a) type-1 transformations and (b) type 2 transformations.

2.5. For the NLE method, the P_{rec} values were higher than 97.6% and the (RMSE $\times$ 100) values were lower than 4. As there are additional experimental sources of error in the system that did not exist in the simulations performed before 8 bits were introduced, the resolution of the results obtained is more limited.

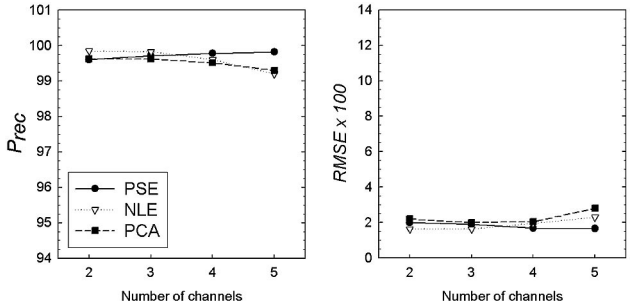

Fig. 17. Experimental results of reconstruction (mean P_{rec} and RMSE) obtained for the whole set of 80 samples with the 12-bit camera and the luminance adaptation model with type 2 transformations.

C. Reconstructions with 12-bit Cameras

In this subsection, we present the reconstruction results obtained by using a Photometrics Sensys KAF0400-G2 camera with 12-bit depth. Figure 16 shows the mean reconstruction parameters obtained for the 19 textile samples. Again, the reconstructions obtained by means of type-1 transformations were limited and similar to those obtained with 8 bits, thus making it highly advisable to use the luminance adaptation with type-2 transformations. In this case, the parameters obtained were almost constant with the number of channels, except for the NLE method for which slightly worse results were observed when more channels were used. The constancy observed in the results can be explained by the smoothness of the reflectances of the 19 samples, which can be reconstructed by use of a small number of spectral bands. The P_{rec} values were higher than 99.8% and the (RMSE $\times$ 100) values were lower than 1.9 when five channels and PSE and

Table 3. Mean, Maximum, and Minimum Values for P_{rec} and RMSE, Obtained for the Whole Set of 80 Samples with the 12-bit Camera and the Luminance Adaptation Model with Transformations 2

Method	Number of filters	2	3	4	5
PSE	Mean P_{rec}	99.605	99.712	99.780	99.820
	Max P_{rec}	99.994	99.997	99.996	99.998
	Min P_{rec}	98.216	97.537	96.350	96.945
	Mean (RMSE $\times$ 100)	2.011	1.913	1.690	1.660
	Max (RMSE $\times$ 100)	5.500	5.836	6.393	6.613
	Min (RMSE $\times$ 100)	0.488	0.268	0.310	0.300
NLE	Mean P_{rec}	99.842	99.828	99.601	99.200
	Max P_{rec}	99.997	99.997	99.997	99.997
	Min P_{rec}	98.030	97.716	96.556	97.378
	Mean (RMSE $\times$ 100)	1.624	1.633	1.950	2.302
	Max (RMSE $\times$ 100)	6.115	6.583	7.163	8.054
	Min (RMSE $\times$ 100)	0.324	0.266	0.276	0.259
PCA	Mean P_{rec}	99.621	99.619	99.515	99.302
	Max P_{rec}	99.994	99.997	99.997	99.997
	Min P_{rec}	98.343	97.527	95.295	95.156
	Mean (RMSE $\times$ 100)	2.201	2.002	2.050	2.800
	Max (RMSE $\times$ 100)	5.535	5.785	7.448	10.681
	Min (RMSE $\times$ 100)	0.531	0.273	0.308	0.339

PCA were used, while the P_{rec} values were higher than 99.3% and the (RMSE $\times$ 100) values were lower than 2.2 with NLE. These results are better than those obtained with 8 bits, so they are closer to the ideal conditions obtained in the simulations, that is, 99.9% for P_{rec} and 1 for RMSE.

Therefore, using the optimal configuration, that is, the 12-bit camera and the luminance adaptation model with type-2 transformations, we reconstructed 80 samples of a wide range of materials. The results obtained are shown in Fig. 17 and Table 3, in which more detailed information is provided. NLE provided very similar reconstructions to those obtained for the 19 textile samples and PSE also gave good results, with a slight improvement as the number of channels increased because of the greater variation in the spectral reflectances of the 80 samples. PCA did not yield satisfactory results. Because of the greater variation in the curves, the principal components used did not, in this case, accurately describe all of the profiles analyzed. This caused the reconstructions of some samples to have poor P_{rec} and RMSE values. In general, because of the amplification of errors with NLE, although it provides quite good results with a relatively small number of channels, and the poorer performance of PCA when many samples are taken into account, the PSE method is preferred. Moreover, with the PSE method no characterization of the system is needed, while with the PCA technique the spectral sensitivity of each multispectral channel must be known, which makes this method more difficult to implement. With PSE, using five channels and taking the 80 samples analyzed into account, we find that the reconstruction parameters have the following mean values: $P_{rec} \geq 99.8\%$, (RMSE $\times$ 100) ≤ 1.7, which are fairly close to the ideal conditions imposed [$P_{rec} \geq 99.9\%$ and (RMSE $\times$ 100) ≤ 1]. To illustrate the reconstructions obtained, several examples are shown in Fig. 18.

4. Conclusions

We performed a complete study of an experimental multispectral system developed to work in the NIR of the electromagnetic spectrum. The system, which was composed of a halogen lamp, five acquisition channels, and a digital CCD camera with an automated zoom lens, was capable of reconstructing the spectral reflectance curves of the samples analyzed between 800 and 1000 nm. The samples considered constituted a representative set, and they all presented typical smooth profiles in the NIR. We also developed a luminance adaptation model to remove the dependence of the multispectral images on the exposure time of the camera and the *f*-number of the objective lens used in the acquisition process. This allowed us to adapt the dynamic range of the camera to the amount of incident light, which depends on the reflectance levels of the sample and on the channel that is used. Specifically, two classes of fittings were applied: one in which the five channels were considered as a whole (type 1) and one in which a different

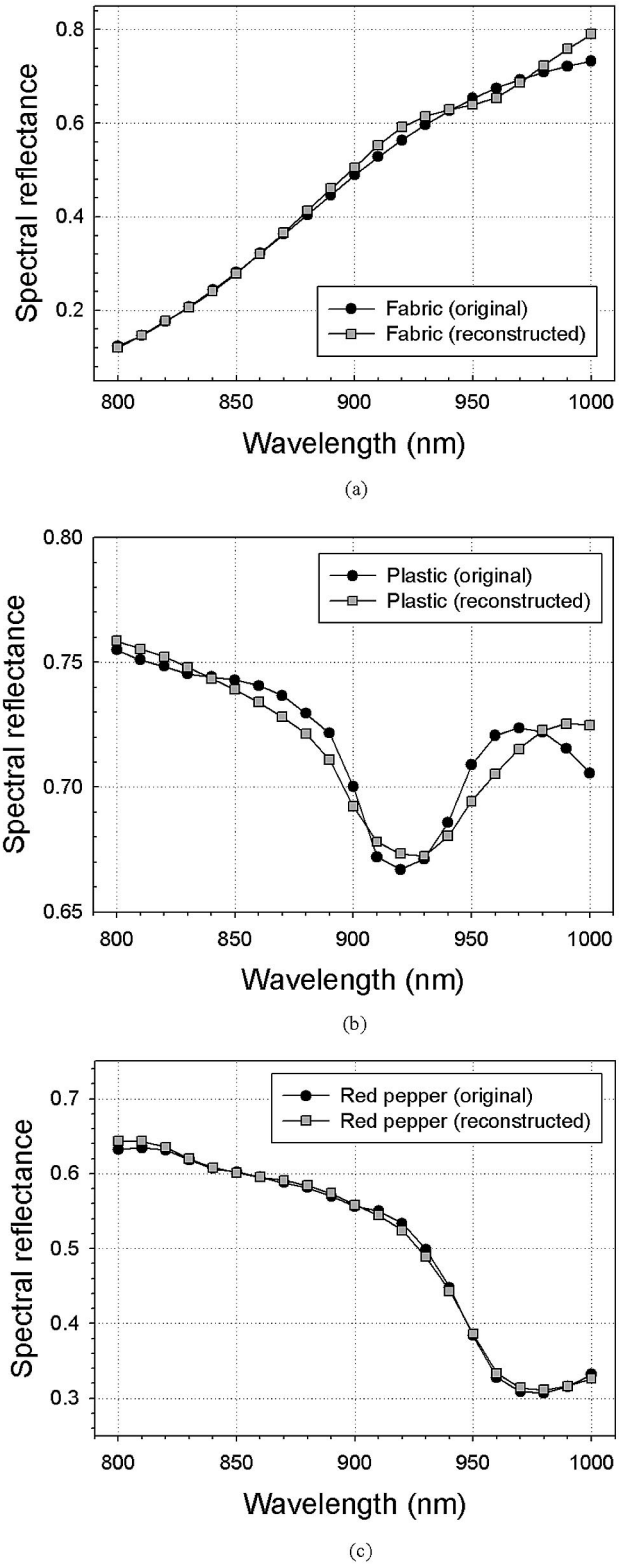

Fig. 18. Measured and reconstructed spectral reflectances for some samples corresponding to an area of 0.5 cm in diameter, obtained with the 12-bit camera and the luminance adaptation model with type 2 transformations: (a) fabric, (b) plastic, and (c) red pepper.

correction was performed depending on the acquisition channel (type 2). Once the images had been corrected by use of the luminance adaptation model, several mathematical reconstruction methods were applied: PSE, NLE, and PCA.

To optimize the reconstruction process, we first analyzed the sources of error found in the system. This involved studying errors resulting from the mechanical positioning, the stability of the illumination, the mathematical approximations performed, and the different kinds of noise introduced by the CCD camera, such as dark current, quantization, and shot noise. Subsequently we compared the experimental results of the reconstruction that we achieved by using CCD cameras with 8- or 12-bit depth for a set of 80 samples with different reflectance spectra in the NIR. The best results were achieved using the pseudoinverse method, the luminance adaptation model with type 2 transformations, and the 12-bit CCD camera. Under these conditions, using five channels, we obtained a mean percentage of reconstruction averaged over the whole set of samples higher than 99.8% and a (RMSE $\times$ 100) value lower than 1.7, which are very close to the ideal ones obtained in the simulations [$P_{\mathrm{rec}} \geq 99.9\%$, (RMSE $\times$ 100) $\leq$ 1]. This demonstrates the capacity of the system we developed to reconstruct the spectral reflectance curves of samples in the NIR region of the electromagnetic spectrum.

This research was supported by the Spanish Ministry for Science and Technology (Ministerio de Ciencia y Tecnología) by means of grant number DP12002-00118. M. Vilaseca thanks the Generalitat (government) of Catalonia for the Ph.D. grant that she received. M. de Lasarte thanks the Spanish Ministry for Education and Science (Ministerio de Educación y Ciencia) for the Ph.D. grant that she received.

References

1. M. Vilaseca, J. Pujol, and M. Arjona, "Spectral-reflectance reconstruction in the near-infrared region by use of conventional charge-coupled-device camera measurements," Appl. Opt. **42,** 1788–1797 (2003).
2. M. Vilaseca, J. Pujol, M. Arjona, and F. M. Martínez-Verdú, "Illuminant influence on the reconstruction of near-infrared spectra," J. Imaging Sci. Technol. **48,** 111–119 (2004).
3. M. Arjona, M. Vilaseca, and J. Pujol, "Multispectral system for recovering near-infrared reflectance spectra," in *Proceedings of the Second European Conference on Colour in Graphics, Imaging and Vision* (CGIV 2004) (The Society for Imaging Science and Technology, 2004), Vol. 1, pp. 409–413.
4. M. Vilaseca, M. Arjona, J. Pujol, and F. M. Martínez-Verdú, "Color visualization system for near-infrared multispectral images," J. Imaging Sci. Technol. **49,** 246–255 (2005).
5. Y. Miyake, "Multispectral imaging: Past, present and future," in *Proceedings of the Tenth Congress of the International Colour Association,* J. L. Nieves and J. Hernández-Andrés, eds., (AIC, 2005), Vol. 1, pp. 477–479.
6. B. Hill, "(R)evolution of color imaging systems," in *Proceedings of the First European Conference on Colour in Graphics, Imaging and Vision* (CGIV 2002) (The Society for Imaging Science and Technology, 2002), Vol. 1, pp. 473–479.
7. F. Schmitt, G. Aitken, G. Alquié, H. Brettel, M. B. Chouikha, P. Colantoni, P. Cotte, J. Cupitt, C. de Deyne, D. Dupraz, C. Lahanier, H. Liang, R. Pilay, A. Ribés, and D. Saunders, "CRISATEL multispectral imaging system," in *Proceedings of the Tenth Congress of the International Colour Association,* J. L. Nieves and J. Hernández-Andrés, eds., (AIC, 2005), Vol. 1, pp. 463–468.
8. R. Berns, "Rejuvenating the appearance of cultural heritage using color and imaging science techniques," in *Proceedings of the 10th Congress of the International Colour Association,* J. L. Nieves and J. Hernández-Andrés, eds., (AIC, 2005), Vol. 1, pp. 369–374.
9. J. Hardeberg and J. Gerhardt, "Characterization of an eight colorant inkjet system for spectral color reproduction," in *Proceedings of the Second European Conference on Colour in Graphics, Imaging and Vision* (CGIV 2004) (The Society for Imaging Science and Technology, 2004), Vol. 1, pp. 263–267.
10. H. Kanazawa, M. Yamaguchi, H. Haneishi, and N. Ohyama, "Natural vision XML database," in *Proceedings of the Tenth Congress of the International Colour Association,* J. L. Nieves and J. Hernández-Andrés, eds., (AIC, 2005), Vol. 2, pp. 1661–1664.
11. N. Tsumura, "Appearance reproduction and multi-spectral imaging," in *Proceedings of the 10th Congress of the International Colour Association,* J. L. Nieves and J. Hernández-Andrés, eds., (AIC, 2005), Vol. 1, pp. 119–123.
12. D. A. Burns and E. W. Ciurczak, *Handbook of Near-Infrared Analysis* (Marcel Dekker, 2001).
13. T. Alexander, and C. D. Tran, "Near-infrared multispectral imaging technique for visualizing sequences of di- and tripeptides synthesized by solid phase combinatorial method," Appl. Spectrosc. **55,** 939–945 (2001).
14. S. Baronti, A. Casini, F. Lotti, and S. Porcinai, "Principal component analysis of visible and near-infrared multispectral images of works of arts," Chemom. Intell. Lab. Syst. **39,** 103–114 (1997).
15. G. C. Holst, *CCD Arrays, Cameras, and Displays* (SPIE Press, 1998).
16. F. M. Martínez-Verdú, J. Pujol, M. Vilaseca, and P. Capilla, "Reproduction model with luminance adaptation for digital cameras," in *Proceedings of the First European Conference on Colour in Graphics, Imaging and Vision* (CGIV 2004) (The Society for Imaging Science and Technology, 2004), Vol. 1, pp. 529–533.
17. M. J. Vrhel and H. J. Trussell, "Filter considerations in color correction," IEEE Trans. Image Process. **3,** 147–161 (1994).
18. P. G. Herzog, D. Knipp, H. Stiebig, and F. König, "Colorimetric characterization of novel multiple-channel sensors for imaging and metrology," J. Electron. Imaging **8,** 342–353 (1999).
19. G. Hong, M. R. Luo, and P. A. Rhodes, "A study of digital camera colorimetric characterization based on polynomial modeling," Color Res. Appl. **26,** 76–84 (2001).
20. F. König, "Reconstruction of natural spectra from a color sensor using nonlinear estimation methods," in *Proceedings of the IS&T Fiftieth Annual Conference* (The Society for Imaging Science and Technology, 1997), pp. 454–458.
21. Y. Hardeberg, F. Schmitt, and H. Brettel, "Multispectral color image capture using a liquid crystal tunable filter," Opt. Eng. **40,** 2532–2548 (2002).
22. F. Imai, and R. S. Berns, "Comparative analysis of spectral reflectance reconstruction in various spaces using a trichromatic camera system," J. Imaging Sci. Technol. **44,** 280–287 (2000).
23. F. H. Imai, M. R. Rosen, and R. S. Berns, "Comparative study of metrics for spectral match quality," in *Proceedings of the First European Conference on Colour in Graphics, Imaging and Vision* (CGIV 2002) (The Society for Imaging Science and Technology, 2002), Vol. 1, pp. 492–496.

24. J. A. S. Viggiano, "Metrics for evaluating spectral matches: A quantitative comparison," in *Proceedings of the Second European Conference on Colour in Graphics, Imaging and Vision* (CGIV 2002) (The Society for Imaging Science and Technology, 2002), Vol. 1, pp. 286–291.
25. J. Y. Hardeberg, "Acquisition and reproduction of color images: Colorimetric and multispectral approaches," Ph.D. thesis (Ecole Nationale Supérieure des Télécommunications, Paris, 1999).
26. G. Sharma, and H. J. Trussell, "Set theoretic estimation in color scanner characterization," J. Electron. Imaging **5,** 479–489 (1996).
27. P. M. Hubel, D. Sherman, and J. E. Farrell, "A comparison of methods of sensor spectral sensitivity estimation," in *Proceedings of Second Color Imaging Conference: Color Science, Systems and Applications* (The Society for Imaging Science and Technology, 1994), pp. 45–48.
28. G. E. Healey, and R. Kondepudy, "Radiometric CCD camera calibration and noise estimation," IEEE Trans. Machine Intell. **16,** 267–276 (1994).
29. Application Note MTD/PS-0233 revision 2.1, "CCD image sensor noise sources," Image Sensor Solutions, Eastman Kodak Company, Rochester, New York (January 2005).